Low-Affinity Signature of the Rat β-Parvalbumin CD Site. Evidence for Remote Determinants†

Michael T. Henzl* and Kelly Ndubuka

Department of Biochemistry, University of Missouri—Columbia, Columbia, Missouri 65211

Received July 14, 2006; Revised Manuscript Received September 17, 2006

ABSTRACT: Although rat β-parvalbumin and chicken parvalbumin 3 (CPV3) are identical at 74 of 108 residues, rat β exhibits perceptibly lower Ca^{2+} and Mg^{2+} affinities. At 25 °C, in Hepes-buffered saline, at pH 7.4, the overall $\Delta\Delta G^{\circ\prime}$ values are 2.0 and 3.9 kcal/mol, respectively. These differences primarily reflect the disparate behavior of the CD sites in the two proteins. Their respective binding constants for Ca^{2+}, for example, are 1.5×10^6 and 2.4×10^7 M^{-1}. The extent to which this differential behavior is dictated by local and remote sequence differences is unknown. To explore this question, we performed mutagenesis on rat β, substituting the corresponding CPV3 codon for residues 49, 50, 57, 58, 59, and 60. The resulting CD site is identical to CPV3 at 27 of 30 positions. The mutations were introduced in four stages, replacing residues 49 and 50 (yielding β 49/50), then 57 and 58 (β 49/50/57/58), then 59 (β 49/50/57/58/59), and finally 60 (β 49/50/57/58/59/60). Apoprotein stability was examined by scanning calorimetry and chemical denaturation and divalent ion affinity by titration calorimetry. All four variants exhibit elevated T_m values and are between 0.13 and 0.39 kcal/mol more stable at 25 °C. Although all four proteins display heightened divalent ion affinity, the increases are small. The maximal $\Delta\Delta G^{\circ\prime}$ values, observed for 49/50/57/58/59/60, are just −0.56 and −0.96 kcal/mol for Ca^{2+} and Mg^{2+}, respectively. Evidently, structural features beyond the metal ion-binding motif contribute to the unusual divalent ion-binding behavior associated with the rat β CD site.

The role of Ca^{2+} in eukaryotic signal transduction (*1*−*3*) is mediated by numerous Ca^{2+}-binding proteins. Many of these belong to the EF-hand family, named for its distinctive metal ion-binding motif (*4*−*6*). First recognized in carp parvalbumin (*7*), the EF-hand includes a central ion-binding loop and flanking helices, the arrangement of which can be mimicked with the right hand. The ligands, positioned at the vertices of an octahedron, are labeled by Cartesian axes: $+x$, $+y$, $+z$, $-y$, $-x$, and $-z$. The $-y$ ligand is a backbone carbonyl; $-x$ is commonly water; and $-z$ is generally glutamate. Side-chain oxygen atoms supply the remaining three ligands.

Certain EF-hand proteins have explicit regulatory roles; others function as cytosolic Ca^{2+} buffers. This diversity has engendered correspondingly diverse divalent ion-binding behavior. High-affinity (Ca^{2+}/Mg^{2+}) sites display Ca^{2+}- and Mg^{2+}-binding constants in excess of 10^7 and 10^4 M^{-1}, respectively. Their low-affinity (Ca^{2+}-specific) counterparts display values of $\approx 10^6$ and $< 10^3$ M^{-1}. The basis for this variation is incompletely understood. We are exploring EF-hand structure−affinity relationships in select members of the parvalbumin (PV[1]) family.

Parvalbumins are small, vertebrate-specific proteins (*8*, *9*). The PV molecule contains six helices, A−F, organized into two domains (Figure 1). The CD-EF metal ion-binding domain (residues 41−108) harbors two EF-hand motifs (the CD and EF sites). The N-terminal AB domain (residues 1−40), a vestigial EF-hand motif, suffered a two-residue deletion that abolished its ion-binding capability. In the Ca^{2+}-bound protein, it packs tightly against the CD-EF domain.

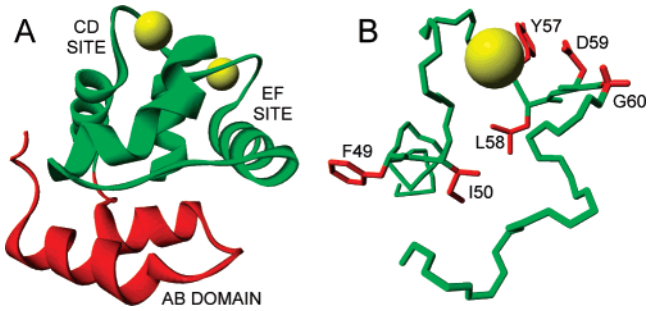

FIGURE 1: Structure of rat β-PV. (A) Ribbon diagram of rat β-PV. The coordinates are from Ahmed et al. (*34*). (B) Close-up of the CD site. The side-chains of the residues mutated in this study are displayed in red. The Figure was prepared with WebLab ViewerLite 3.20 (Molecular Simulations, Inc.).

The PV family includes α and β sub-lineages (*10*, *11*). Mammals express one PV from each lineage (*12*). Although generally viewed as cytosolic Ca^{2+} buffers, certain isoforms

† This work was supported by NSF awards MCB0131166 and MCB0543476 (to M.T.H.).

* Corresponding author. Tel: 573-882-7485. Fax: 573-884-4812. E-mail: henzlm@missouri.edu.

[1] Abbreviations: ATH, avian thymic hormone; CD, circular dichroism; CD site, parvalbumin metal ion-binding site flanked by the C and D helical segments; CPV3, chicken parvalbumin 3; DMPC, dimyristoylphosphatidylcholine; DPPC, dipalmitoylphosphatidylcholine; DSPC, distearoylphosphatidylcholine; EDTA, ethylenediaminetetraacetic acid; EF site, parvalbumin metal ion-binding site flanked by the E and F helical segments; EGTA, ethylene glycol-bis(β-aminoethyl ether)-*N*,*N*,*N*′,*N*′-tetraacetic acid; Hepes, 4-(2-hydroxyethyl)-1-piperazineethanesulfonic acid; ITC, isothermal titration calorimetry; LB, Luria−Bertani; NTA, nitrilotriacetic acid; PAGE, polyacrylamide gel electrophoresis; PV, parvalbumin.

10.1021/bi061421h CCC: $37.00
Published on Web 12/14/2006

evidently play more specialized roles. The avian β parvalbumins, avian thymic hormone (ATH) and parvalbumin 3 (PV3), influence T-cell differentiation and proliferation (*13*, *14*). Recently, Yin et al. demonstrated that the mammalian β isoform, also known as oncomodulin, is secreted by activated macrophages and stimulates axonal elongation in retinal ganglion cells (*15*).

Early binding studies (*16*, *17*) suggested that the parvalbumin CD and EF sites were invariably high-affinity sites. It is now apparent that the β sub-lineage exhibits a spectrum of divalent ion affinity, with ATH and the mammalian β isoform representing high- and low-affinity extremes, respectively. The attenuated divalent ion affinity of rat β-PV has been a focus of this laboratory in recent years. An explanation for this behavior could advance our understanding of EF-hand structure−affinity relationships.

Divalent ion-binding data for chicken PV3 (CPV3) suggested a novel strategy for probing this issue (*18*). Although CPV3 and rat β exhibit 69% sequence identity (*19*), CPV3 displays substantially higher Ca^{2+} affinity. The combination of sequence similarity and functional diversity could expedite the search for determinants of divalent ion affinity in the rat β-PV isoform. This article explores the consequences of performing rat $\beta \rightarrow$ CPV3 mutations at residues 49, 50, 57, 58, 59, and 60. The resulting CD site is identical to that in CPV3 at 27 of 30 residues, and the remaining three nonidentities reflect conservative sequence substitutions.

MATERIALS AND METHODS

Materials. LB agar, LB broth, ampicillin, NaCl, Hepes, $CaCl_2 \cdot 2H_2O$, $MgCl_2 \cdot 2H_2O$, sodium phosphate, $Na_2EDTA \cdot 2H_2O$, lysozyme, Spectrapor 1 dialysis tubing, *N*,*N*′-methylene-bis-acrylamide, and acrylamide were purchased from Fisher Scientific Co. DEAE-Sepharose, Sephadex G-75, and ultrapure urea (Fluka) were obtained from Sigma-Aldrich Co.

Protein Expression and Purification. The rat β expression vector, pLD2, was derived from pBluescript (Stratagene). Mutagenesis was performed with the Quik-Change mutagenesis kit (Stratagene), using oligonucleotides from Integrated DNA Technologies (Coralville, IA). The fidelity of the resulting sequences was confirmed by automated DNA sequencing.

Proteins were expressed constitutively in *E. coli* DH5α, at 37 °C, in LB broth cultures containing ampicillin (100 μg/mL). The isolation protocol, identical to that of wild-type β, is described elsewhere (*20*). Purity, judged by the A_{274}/A_{290} ratio, exceeded 98% for all preparations.

Protein concentrations were determined by absorbance at 274 nm. Extinction coefficients were measured in a Beckman XL-I analytical ultracentrifuge, employing a synthetic boundary cell. Upon acceleration to 5,000 rpm, the cell produces a sharp solvent−sample interface, which is examined by interference optics and UV absorbance. The deformation of the interference pattern at the interface yields the mass concentration, 3.333 fringes corresponding to a protein concentration of 1.0 mg/mL in a 1.2 cm cell (*21*). The following extinction coefficient estimates were obtained by dividing the A_{274} value by the calculated molar concentration and by 1.2 cm: wild-type β, 2880 M^{-1} cm^{-1}; 49/50, 2970 M^{-1} cm^{-1}; 49/50/57/58, 1708 M^{-1} cm^{-1}; 49/50/57/58/59, 1650 M^{-1} cm^{-1}; and 49/50/57/58/59/60, 1600 M^{-1} cm^{-1}.

Prior to divalent ion-binding measurements, residual Ca^{2+} was removed from the protein preparations by treatment with EDTA-derivatized agarose (*22*, *23*) in 0.15 M NaCl and 0.025 M Hepes at pH 7.4, as described elsewhere (*24*, *25*). The resulting solutions contained less than 0.02 mol equiv of Ca^{2+}, as judged by flame atomic absorption spectrometry.

Isothermal Titration Calorimetry (ITC). ITC was performed in a MicroCal VP-ITC at 25 °C. Samples were titrated with Ca^{2+} in the presence and absence of competitive chelators or Mg^{2+} and with Mg^{2+} in the presence and absence of EDTA. Integrated data from these titrations were subjected to global nonlinear least-squares minimization, yielding binding parameters for both Ca^{2+} and Mg^{2+}. Parameter uncertainties were evaluated by confidence interval analysis and Monte Carlo simulations. The treatment of data is described in detail elsewhere (*26*, *27*).

Differential Scanning Calorimetry (DSC). DSC was performed in a Nano-DSC (Calorimetry Sciences Corporation), equipped with 0.32 mL cylindrical hastalloy cells. Temperature calibration was examined with DMPC, DPPC, and DSPC, using the published transition temperatures (*28*). The accuracy of the differential power measurements was verified with internally generated electrical calibration pulses.

Samples were dialyzed against 0.15 M NaCl, 0.01 M NaPi, and 0.005 M EDTA at pH 7.4, which then served as the reference buffer. Data was collected at 60°/h. Each protein included in the study exhibited an endotherm on rescan, indicating that denaturation was reversible.

A baseline, obtained with sample and reference cells filled with buffer, was subtracted from the protein data prior to analysis. The resulting heat capacity data, c_p, with units of mcal/K, were analyzed with the following model.

$$c_p = \left(\frac{10^3 mc \cdot V}{MW}\right)\left([\Delta H_c(T_m) + \beta\Delta C_p(T - T_m)]\left[\frac{\Delta H_{vH}(T_m) + \Delta C_p(T - T_m)}{RT^2}\right]\left(\frac{K(T)}{(1 + K(T))^2}\right) + \left(\frac{K(T)}{1 + K(T)}\right)\Delta C_p + c_{p,n} + \left(\frac{1}{1 + K(T)}\right)(b \cdot (T - T_m)) + \left(\frac{K(T)}{1 + K(T)}\right)(d \cdot (T - T_m))\right) \quad (1)$$

In this equation, the derivation of which is described in detail elsewhere (*29*), *mc* is the protein concentration in g/L, *V* is the sample cell volume in L, *MW* is the protein molecular weight, β is the ratio of the calorimetric and van't Hoff enthalpies (ΔH_c and ΔH_{vH}, respectively), ΔC_p is the change in heat capacity that accompanies denaturation (assumed to be temperature-independent), *T* is the absolute temperature, T_m is the melting point or transition mid point, and *R* is the gas constant. $K(T)$ is the temperature-dependent equilibrium constant

$$K(T) = \exp(-\Delta G(T)/RT) \quad (2)$$

where $\Delta G(T)$ is given by the Gibbs−Helmholtz equation:

$$\Delta G(T) = \Delta H\left(\frac{T_m - T}{T_m}\right) + \Delta C_p\left[(T - T_m) - T \ln \frac{T}{T_m}\right] \quad (3)$$

For a two-state transition, the fractions of native and

denatured material equal $1/(1 + K(T))$ and $K(T)/(1 + K(T))$, respectively.

The first two terms in eq 1 describe the peak in the heat capacity function and the accompanying baseline shift, respectively. The third term, $c_{p,n}$, represents the value of the native state heat capacity at the T_m, and the remaining two terms describe the temperature dependence of the native and denatured state heat capacities, respectively.

Weighted least-squares analyses were performed in Origin, assuming a uniform standard deviation of 0.003 mcal/K. To improve the estimates for ΔH_c and ΔC_p, data collected at three protein concentrations were modeled simultaneously. T_m, ΔH_c, ΔH_{vH}, and ΔC_p were treated as global variables and allowed to float. $c_{p,n}$, b, and d should likewise be global parameters. However, because of baseline irreproducibility, they were treated as local parameters and allowed to float. Protein concentrations were fixed at the spectroscopically determined values. After obtaining the optimized parameter set and associated minimal chi-square value, parameter uncertainties were investigated by confidence interval analysis, as described elsewhere (*26*, *27*).

Urea Denaturation. Urea denaturation was monitored by circular dichroism (CD) at 222 nm with an AVIV Model 62DS spectrometer. Protein samples (5 μM) were dialyzed against PBS/EDTA buffer (0.15 M NaCl, 0.01 M NaPi, and 0.001 M EDTA at pH 7.4). The 10.0 M urea titrant was prepared by quantitatively transferring 60.06 g of urea to a calibrated 100 mL volumetric flask and then adding 10.0 mL of 10× PBS/EDTA and sufficient water to dissolve the urea. After dilution to 100 mL, the pH was adjusted to pH 7.4. The concentration was confirmed by refractometry. Aliquots of the resulting solution, stored at −20 °C, were thawed once, then discarded.

Urea titrations were performed at 20, 25, 30, and 35 °C, using a Hamilton Microlab 500 auto-titration accessory interfaced with the CD spectrometer. Experiments were conducted in 10 mm cuvets, in a constant 2.0 mL volume. Each urea addition was followed by a 60 s equilibration period and 30 s of data collection. Facile reversibility of the urea-induced denaturation was indicated by the equality of the CD signals obtained by mixing (1) equal volumes of 6.0 M urea and native protein solution and (2) equal volumes of buffer and denatured (6.0 M urea) protein.

The ellipticity data, corrected for dilution, were fit to eq 4 (*30*)

$$y = \frac{(y_n + m_n[\text{urea}]) + (y_u + m_u[\text{urea}]) \times \exp(-(\Delta G_o - m[\text{urea}])/RT)}{1 + \exp(-(\Delta G_o - m[\text{urea}])/RT)} \quad (4)$$

where m_n and y_n are the slope and intercept, respectively, for the pre-transition baseline; y_u and m_u are the slope and intercept, respectively, for the post-transition baseline; ΔG_o is the free energy change for unfolding in the absence of urea; and m describes the sensitivity of the conformational free energy to urea concentration.

To obtain an alternative estimate for ΔC_p, independent of DSC, data collected at the four temperatures were globally fit to eq 4. Rather than treating ΔG_o as a fitting parameter, its value was calculated with the Gibbs−Helmholtz equation, eq 3 (*31*). y_n, m_n, y_u, and m_u were treated as local parameters, unique to each dataset. In principle, m should be a global parameter. However, a significantly lower chi-square value was obtained by treating it as a local parameter. For all of the proteins except β 49/50, a monotonic decrease in m was observed with increasing temperature (Table 5). Because the m value reflects the change in solvent-accessible apolar surface area on denaturation (*32*), it is reasonable that it might decrease with increasing temperature and increased solvent penetration of the native state. The T_m and ΔH_{vH} in eq 3 were fixed at the values determined by DSC. ΔC_p was treated as a global fitting parameter.

RESULTS

Residues 49, 50, 57, 58, 59, and 60 of rat β-PV were replaced with the corresponding residues in CPV3. The mutagenesis was conducted in four stages, first replacing residues 49 and 50 and adding the mutations at residues 57 and 58, then residue 59, and finally residue 60. For clarity, a shorthand notation is used to identify the variant proteins. Thus, 49/50/57/58/59/60 denotes the β variant harboring the F49I, I50L, Y57F, L58I, D59E, and G60E mutations.

Divalent Ion-Binding Properties. The EF-hand motifs in wild-type rat β exhibit distinct divalent ion-binding behaviors (*20*, *27*, *33*). The EF site binds Ca^{2+} with a microscopic binding constant of 2.30×10^7 M^{-1} and an enthalpy of −4.10 kcal/mol. The CD site values are 1.52×10^6 M^{-1} and −3.46 kcal/mol. The EF site binds Mg^{2+} with a binding constant of 9.23×10^3 M^{-1} and an enthalpy of 3.01 kcal/mol. Corresponding CD site numbers are 1.68×10^2 M^{-1} and 4.16 kcal/mol.

The Ca^{2+}- and Mg^{2+}-binding properties of the four rat $\beta \rightarrow$ CPV3 variants were examined by global least-squares analysis of ITC data. This strategy returns parameter estimates for both Ca^{2+} and Mg^{2+}. The suite of experiments employed in this study included direct titrations with Ca^{2+} and Mg^{2+}, titrations with Ca^{2+} in the presence of Mg^{2+} or competing chelators (EDTA, EGTA, NTA), and titrations with Mg^{2+} in the presence of EDTA. Table 1 lists the resulting binding constants and enthalpies for Ca^{2+} and Mg^{2+}. These analyses assume that the CD site retains its low-affinity signature in the variant proteins, that is, that k_1 and k_2 correspond to the EF and CD binding events, respectively. Table 2 summarizes the divalent ion-binding energetics. Figure 9 (panels B−D) presents the $\Delta\Delta G$, $\Delta\Delta H$, and $-T\Delta\Delta S$ values in graphical format.

Raw data for representative titrations with Ca^{2+} are displayed in Figure 3. Data were collected on wild-type β, the four β variants, and CPV3, at concentrations ranging between 60 and 67 μM. The impact of the mutations is particularly evident in the titrations of 49/50/57/58/59 and 49/50/57/58/59/60. The former appears to end prematurely, and the latter displays a pronounced endothermic component.

F49I/I50L. Integrated data for the analysis of β 49/50 are included in the Supporting Information (Figure S1). Least-squares minimization of the composite dataset reveals that the combined mutations produce a perceptible elevation in Ca^{2+} affinity. Both binding constants are increased, to 3.19×10^7 and 2.26×10^6 M^{-1}, respectively, for a 0.42 kcal/mol improvement in Ca^{2+}-binding free energy. Because both binding enthalpies are less exothermic than that in the wild-type protein, the more favorable binding free energy evidently has an entropic origin.

Table 1: Divalent Ion-Binding Properties

	Ca^{2+} values				Mg^{2+} values			
protein	k_1[a] M^{-1}	H_1 kcal/mol	k_2[a] M^{-1}	H_2 kcal/mol	k_{1M}[a] M^{-1}	H_{1M} kcal/mol	k_{2M}[a] M^{-1}	H_{2M} kcal/mol
β-PV[b]	2.30×10^7	−4.10	1.52×10^6	−3.46	9.23×10^3	3.01	1.68×10^2	4.16
	(2.05, 2.56)	(−4.16, −4.06)	(1.38, 1.70)	(−3.52, −3.41)	(8.93, 9.66)	(2.97, 3.05)	(1.58, 1.79)	(4.00, 4.32)
var1[c]	3.19×10^7	−3.51	2.26×10^6	−3.22	1.34×10^4	4.22	1.46×10^2	5.42
	(2.57, 3.80)	(−3.70, −3.31)	(1.90, 2.92)	(−3.42, −3.01)	(1.17, 1.57)	(3.98, 4.53)	(1.20, 1.66)	(5.00, 6.16)
var2[c]	4.29×10^7	−3.78	1.45×10^6	−3.38	1.79×10^4	3.39	3.34×10^2	4.26
	(3.73, 4.68)	(−3.89, −3.66)	(1.31, 1.60)	(−3.28, −3.48)	(1.65, 1.95)	(3.29, 3.52)	(2.80, 3.74)	(4.04, 4.47)
var3[c]	4.65×10^7	−4.92	1.70×10^6	0.16	1.92×10^4	2.50	5.09×10^2	5.34
	(4.42, 4.89)	(−5.02, −4.82)	(1.64, 1.77)	(0.12, 0.19)	(1.82, 2.05)	(2.38, 2.57)	(4.68, 5.44)	(5.13, 5.56)
var4[c]	3.76×10^7	−3.98	2.43×10^6	2.56	1.60×10^4	3.34	4.91×10^2	5.78
	(3.46, 4.45)	(−4.24, −3.84)	(2.28, 2.88)	(2.43, 2.74)	(1.53, 1.96)	(2.91, 3.55)	(4.58, 7.41)	(5.31, 6.19)
CPV3[d]	4.50×10^7	−5.46	2.43×10^7	−0.13	4.98×10^4	1.53	2.12×10^4	1.62
	(4.31, 4.96)	(−5.68, −5.30)	(2.36, 2.66)	(−0.21, −0.04)	(4.74, 5.79)	(1.31, 1.62)	(1.94, 2.38)	(1.30, 1.76)

[a] Microscopic binding constants are shown with uncertainties (68% confidence intervals) parentheses. [b] Values are from ref 27 (*27*). [c] Var1 is the abbreviation for the 49/50 variant; var2 denotes 49/50/57/58; var3 corresponds to 49/50/57/58/59; and var4 represents 49/50/57/58/59/60/59/60. [d] Values are from ref 18 (*18*).

Table 2: Divalent Ion-binding Energetics[a]

	Ca^{2+} binding			Mg^{2+} binding		
protein	ΔG[b]	ΔH	$-T\Delta S$[c]	ΔG[b]	ΔH	$-T\Delta S$[c]
			EF Site			
rat β-PV	−10.04	−4.10	−5.94	−5.41	3.01	−8.42
49/50	−10.23	−3.51	−6.72	−5.63	4.22	−9.85
49/50/57/58	−10.41	−3.78	−6.63	−5.80	3.39	−9.19
49/50/57/58/59	−10.45	−4.92	−5.53	−5.84	2.50	−8.34
49/50/57/58/59/60	−10.33	−3.98	−6.35	−5.73	3.34	−9.07
CPV3	−10.43	−5.46	−4.97	−6.40	1.53	−7.93
			CD Site			
rat β-PV	−8.43	−3.46	−4.97	−3.03	4.16	−7.19
49/50	−8.66	−3.22	−5.44	−2.95	5.42	−8.37
49/50/57/58	−8.40	−3.38	−5.02	−3.44	4.26	−7.70
49/50/57/58/59	−8.49	0.16	−8.65	−3.69	5.34	−9.03
49/50/57/58/59/60	−8.71	2.56	−11.27	−3.67	5.78	−9.45
CPV3	−10.07	−0.13	−9.94	−5.90	1.62	−7.52
			Overall			
rat β-PV	−18.47	−7.56	−10.91	−8.44[e]	7.17	−15.61
49/50	−18.89	−6.73	−12.16	−8.58	9.64	−18.22
49/50/57/58	−18.81	−7.16	−11.65	−9.24	7.65	−16.89
49/50/57/58/59	−18.95	−4.76	−14.19	−9.53	7.84	−17.37
49/50/57/58/59/60	−19.03	−1.42	−17.61	−9.40	9.12	−18.52
CPV3	−20.50	−5.59	−14.91	−12.30	3.15	−15.45

[a] Energies are expressed in kcal/mol. All binding data were collected in Hepes-buffered saline at pH 7.4 at 25 °C. [b] Equal to $-RT \ln k_1k_2$, where R is the gas constant, T is the absolute temperature, and k_1 and k_2 are the microscopic binding constants for the first and second binding events, respectively. [c] Equal to $\Delta G - \Delta H$.

The mutations have a smaller impact on Mg^{2+} affinity. Although the binding constant for the EF site increases to 1.34×10^4 M^{-1}, the CD site value decreases slightly to 1.46×10^2 M^{-1}. As a result, the $\Delta\Delta G$ is just −0.14 kcal/mol. Both Mg^{2+}-binding enthalpies become more endothermic with the replacement of residues 49 and 50, the EF-site value increasing by 1.21 kcal/mol and the CD site value increasing by 1.26 kcal/mol. This result suggests, as remarked for Ca^{2+}, that the entropic contribution to Mg^{2+} binding is substantially more favorable for the 49/50 variant.

F49I/I50L/Y57F/L58I. The 49/50/57/58 variant also exhibits perceptibly higher affinity for Ca^{2+}. The integrated ITC data are included in the Supporting Information (Figure S2). Although the improvement in overall binding free energy ($\Delta\Delta G = -0.34$ kcal/mol), relative to that of wild-type β, is similar to that observed for β 49/50 (i.e., −0.42 kcal/mol), the increase in affinity is evidently associated with the first binding event. Whereas the introduction of Y57F and L58I into the β 49/50 background increases the EF-site Ca^{2+}-binding constant from 3.19×10^7 to 4.29×10^7, the CD site constant decreases from 2.26×10^6 to 1.45×10^6 M^{-1}.

Although 49/50 and 49/50/57/58 have comparable overall Ca^{2+} affinity, the latter has significantly higher affinity for Mg^{2+}. The overall improvement in Mg^{2+} affinity, relative to wild-type β, is 0.80 kcal/mol, compared to 0.14 kcal/mol for 49/50. Least-squares analysis suggests that the Mg^{2+} binding constants for both sites have increased significantly, to 1.79×10^4 for the EF site and 3.34×10^2 M^{-1} for the CD site.

F49I/I50L/Y57F/L58I/D59E. The direct titration of this protein with Ca^{2+} can be accommodated by a single-site model with an apparent binding constant of 5.7×10^5 M^{-1}. In fact, the protein contains two functional Ca^{2+}-binding sites, but the ΔH associated with the second binding event is small, rendering it effectively invisible. In the global analysis (Figure 4), however, the site is detected by its impact on competing equilibria. It is most clearly evident when the protein is titrated with Ca^{2+} in the presence of NTA (Figure 4A, □ and △). Although less obvious in Ca^{2+} titrations in the presence of Mg^{2+}, EDTA, or EGTA, satisfactory modeling of these data requires the assumption of two sites having Ca^{2+}-binding constants of 4.65×10^7 and 1.70×10^6 M^{-1}.

The least-squares analysis suggests that the introduction of the D59E mutation into 49/50/57/58 produces a change in overall Ca^{2+} affinity of −0.14 kcal/mol. This modest change in ΔG notwithstanding, the binding enthalpies have

```
          1                   10                  20                  30
RAT β   S I T D I L S A E D I A A A L Q E C Q D P D T F E P Q K F F Q T S G L S K M
CPV3    - L - - - - - P S - - - - - - - R D - - A - - S - S - K - - - - I - - M - - K

            40                  50                  60                  70
RAT β   S A S Q V K D I F R F I D N D Q S G Y L D G D E L K Y F L Q K F Q S D A R E
CPV3    - S - - L - E - - - I L - - - - - - - F I E E - - - - - - - - - R - E - G - - V

                80                  90                  100
RAT β   L T E S E T K S L M D A A D N D G D G K I G A D E F Q E M V H S
CPV3    - - A - - - - T F L A - - - H - - - - - - - - E - - - - - - Q -
```

FIGURE 2: Amino acid sequences of rat β-PV and the C72S variant of CPV3. Data are from references 46 (*46*) and 19 (*19*), respectively.

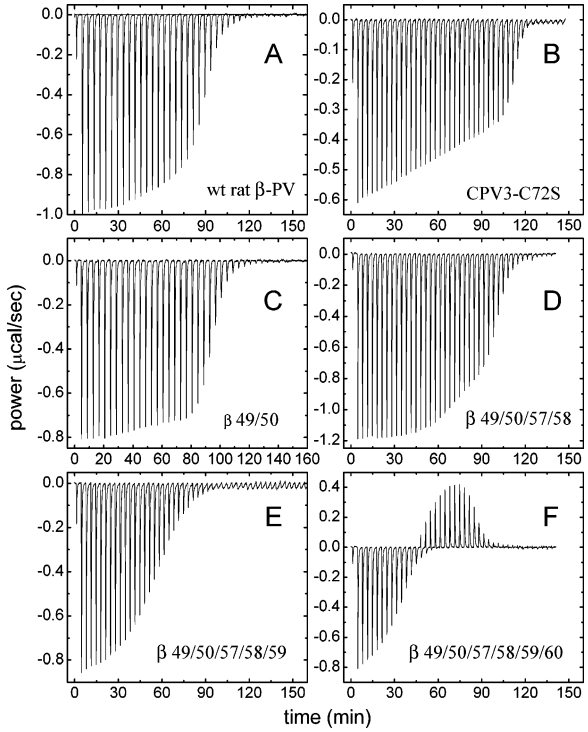

FIGURE 3: Raw ITC data. Representative titrations with Ca^{2+}. (A) 1.0 mM Ca^{2+} vs 60 μM wild-type rat β-PV. (B) 1.0 mM Ca^{2+} vs 60 μM CPV3-C72S. (C) 1.0 mM Ca^{2+} vs 63 μM β 49/50. (D) 1.0 mM Ca^{2+} vs 65 μM β 49/50/57/58. (E) 1.0 mM Ca^{2+} vs 67 μM β 49/50/57/58/59. (F) 1.0 mM Ca^{2+} vs 63 μM β 49/50/57/58/59/60.

undergone marked alteration, with $\Delta\Delta H$ values for the EF and CD sites of -1.14 and 3.54 kcal/mol, respectively.

The free energy change associated with Mg^{2+} binding is 0.29 kcal/mol more favorable than that for 49/50/57/58. Most of this change is attributable to an increase in the CD site binding constant from 3.34×10^2 to 5.09×10^2. The EF site value is nearly unchanged at 1.92×10^4 M^{-1}. As observed for Ca^{2+}, the binding enthalpy is more favorable ($\Delta\Delta H = -0.89$ kcal/mol) for the EF site and less favorable ($\Delta\Delta H = 1.08$ kcal/mol) for the CD site.

F49I/I50L/Y57F/L58I/D59E/G60E. Figure 5 presents ITC data for β 49/50/57/58/59/60. As noted above, the titration of this protein with Ca^{2+} is remarkable for the endothermic nature of the second binding event. Although we have previously observed endothermic Ca^{2+} binding events in PV variants (*25*), those proteins displayed markedly attenuated divalent ion affinity. In this instance, the overall Ca^{2+} affinity of 49/50/57/58/59/60 is 0.56 kcal/mol more favorable than that of wild-type β, and the overall Mg^{2+} affinity is 0.96 kcal/mol more favorable.

Least-squares analysis indicates that the introduction of G60E into 49/50/57/58/59 reduces the EF-site binding constant from 4.65×10^7 to 3.76×10^7 M^{-1} and increases the CD site affinity from 1.70×10^6 to 2.43×10^6. These compensating changes leave the overall ΔG nearly unchanged ($\Delta\Delta G = -0.08$ kcal/mol). As with 49/50/57/58/59, the negligible free energy change is the result of large, opposing changes in binding enthalpy and entropy. The $\Delta\Delta H_{Ca}$ values for the EF and CD sites are 0.94 and 2.40 kcal/mol, respectively. With respect to Mg^{2+} binding, the mutation slightly lowers affinity at both binding sites, affording an overall $\Delta\Delta G$ of 0.13 kcal/mol. The $\Delta\Delta H_{Mg}$ values for the EF and CD sites are 0.84 and 0.44 kcal/mol, respectively.

Differential Scanning Calorimetry. Figure 6A displays the molar heat capacities of the wild-type and variant proteins. All four variants exhibit perceptibly higher melting temperatures, with ΔT_m values ranging from 1.9° to 3.4°. For each protein, denaturation data were acquired at three concentrations and subjected to simultaneous least-squares minimization to extract estimates for T_m, ΔH_c, ΔH_{vH}, and ΔC_p. Table 3 lists the resulting values.

Denaturation data for wild-type β, displayed in Figure 6B, were collected at protein concentrations of 2.25(△), 4.49 (□), and 6.73 (○) mg/mL. Under these solution conditions, the observed T_m is 49.3 °C. Simultaneous least-squares analysis of the datasets yielded values for ΔH_c, ΔH_{vH}, and ΔC_p of 72.9 kcal/mol, 67.9 kcal/mol, and 1.60 kcal mol^{-1} K^{-1}, respectively. Figure 6C displays DSC data for β 49/50, collected at concentrations of 4.66 (△), 6.95 (□), and 8.77 (○) mg/mL. The combined F49I and I50L mutations increase the calorimetric enthalpy of wild-type rat β by approximately 14 kcal/mol, from 72.9 to 86.6 kcal/mol. However, the van't Hoff enthalpy, at 69.9 kcal/mol, exhibits a much smaller increase ($\Delta\Delta H_{vH} = 2.0$ kcal/mol). There is an apparent increase in ΔC_p, from 1.60 to 1.76 kcal mol^{-1} K^{-1}.

Figure 6D presents DSC data for β 49/50/57/58, acquired at concentrations of 4.38 (△), 5.75 (□), and 6.94 (○) mg/mL. Global least-squares minimization of the three datasets indicated that introduction of the Y57F and L58I mutations into β 49/50 decreases the T_m by 1.5°, leaves ΔH_c nearly unchanged, reduces ΔH_{vH} by 3.9 kcal/mol, and raises the apparent ΔC_p for denaturation to 1.98 kcal mol^{-1} K^{-1}.

Figure 6E displays DSC data for 49/50/57/58/59 at sample concentrations of 3.79 (△), 5.06 (□), and 6.25 (○) mg/mL. Least-squares analysis suggests that the replacement of Asp-59 by glutamate, in the 49/50/57/58 background, raises the T_m by 0.4°, leaves ΔH_c essentially unchanged, increases ΔH_{vH} by 2.3 kcal/mol, and decreases ΔC_p from 1.98 to 1.74 kcal mol^{-1} K^{-1}. Figure 6F presents DSC data for 49/50/57/58/59/60, collected at protein concentrations of 3.29 (△), 5.61

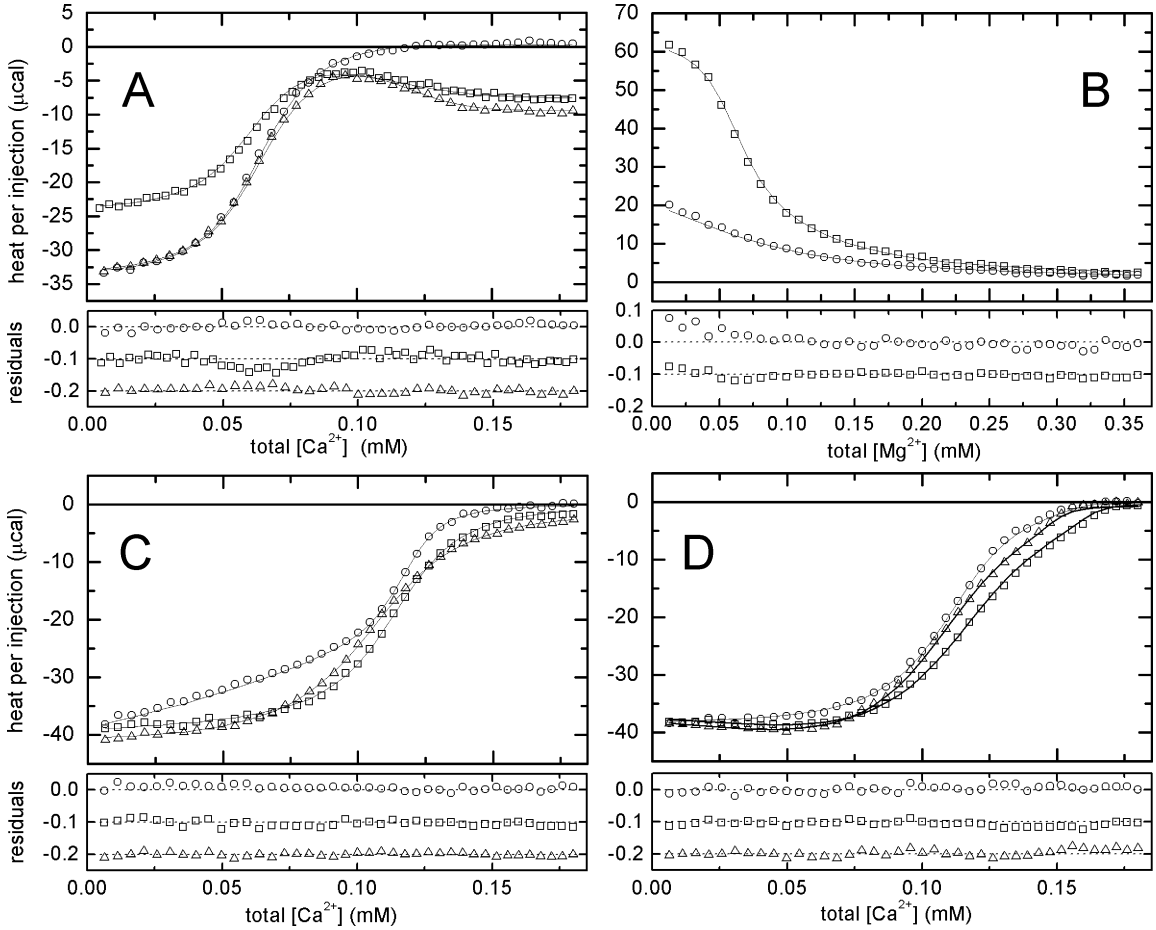

FIGURE 4: Divalent ion-binding behavior of β 49/50/57/58/59. The solid lines represent the best fit to the composite dataset ($\chi_r^2 = 1.55$). The residuals are displayed in the lower panels. (A) 1.0 mM Ca^{2+} vs 67 μM protein (○); 1.0 mM Ca^{2+} vs 63 μM protein and 1.0 mM NTA (□); 1.0 mM Ca^{2+} vs 66 μM protein and 0.5 mM NTA (△). (B) 1.8 mM Mg^{2+} vs 69 μM protein (○); 1.8 mM Mg^{2+} vs 69 μM protein and 100 μM EDTA (□). (C) 1.0 mM Ca^{2+} vs 69 μM protein and 1.0 mM Mg^{2+} (○); 1.0 mM Ca^{2+} vs 69 μM protein and 5.0 mM Mg^{2+} (□); 1.0 mM Ca^{2+} vs 65 μM protein and 10.0 mM Mg^{2+} (△). (D) 1.0 mM Ca^{2+} vs 69 μM protein and 60 μM EDTA (○); 1.0 mM Ca^{2+} vs 64 μM protein and 60 μM EGTA (□);1.0 mM Ca^{2+} vs 60 μM protein and 60 μM EGTA (△).

(□), and 7.76 (○) mg/mL. An analysis of these data indicates that the substitution of glutamate for Gly-60 in 49/50/57/58/59 lowers the T_m by 0.4°, decreases ΔH_c by 0.2 kcal/mol, raises ΔH_{vH} by 3.9 kcal/mol, and decreases ΔC_p from 1.74 to 1.70 kcal mol^{-1} K^{-1}.

The DSC studies suggest that the mutations produce significant changes in ΔC_p, which in turn impact the projected stabilities at 25 °C. Figure 7A displays the stability curves obtained with eq 3, using the DSC-derived estimates of T_m, ΔH_{vH}, and ΔC_p. The curves for the five proteins diverge significantly at lower temperatures, a reflection of the variations in ΔC_p. In particular, although 49/50/57/58 has a higher T_m than that of wild-type β, it is projected to be 0.43 kcal/mol less stable at 25 °C. This prediction was tested by chemical denaturation measurements.

Urea Denaturation. Each protein was titrated with urea at 25 °C, monitoring denaturation by CD. Figure 8A displays the data and optimal least-squares fits. The extrapolated stabilities at zero urea concentration, that is, ΔG_o, are listed in Table 4, along with the corresponding *m* values. Interestingly, the stabilities are more similar than those predicted by DSC. Moreover, the urea denaturation experiment suggests that 49/50/57/58 is actually more stable than wild-type β, not less. This finding cast doubt on the validity of the DSC-derived ΔC_p values.

To clarify this issue, urea titrations were conducted at 20, 25, 30, and 35 °C. The data were simultaneously modeled with eq 4, using the Gibbs−Helmholtz relationship (eq 3) to calculate ΔG_o at each temperature. The T_m and ΔH_{vH} values employed for that calculation were obtained from the corresponding DSC analysis; and ΔC_p was varied to obtain the best agreement with the composite dataset (*31*). Figure 8 (panels B−F) displays the data and optimal least-squares fits. Table 5 lists the resulting ΔC_p estimates, which are substantially lower and more uniform than those obtained by DSC. These values were used, in conjunction with the T_m and ΔH_{vH} values from the DSC studies, to generate the protein stability curves displayed in Figure 7B. Notice that the curves cluster more tightly than those in Figure 7A and are perceptibly shallower.

DISCUSSION

The CD site of the mammalian β-PV exhibits low divalent ion affinity. This study exploits the sequence similarity between rat β and CPV3 to explore this issue. Although the two proteins are identical at 74 of the 108 residues, their apparent overall ΔG values for Ca^{2+} and Mg^{2+} binding differ by 2.03 and 3.86 kcal/mol, respectively (Table 2). These discrepancies largely reflect the disparate binding properties of the CD sites. To what extent are the behaviors of the two

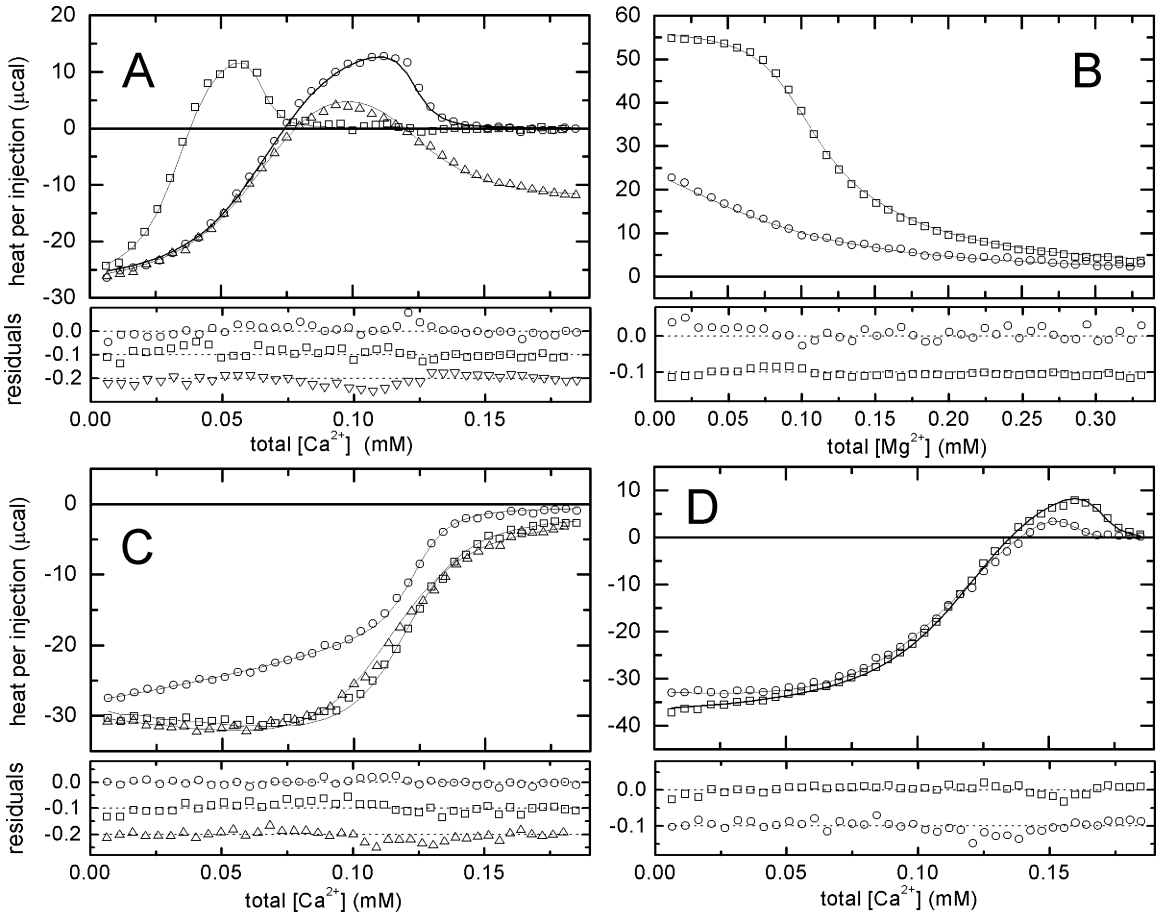

FIGURE 5: Divalent ion-binding behavior of β 49/50/57/58/59/60. The solid lines depict the best fit to the composite dataset ($\chi_r^2 = 3.03$). The lower panels display the residuals for the individual experiments. (A) 1.0 mM Ca^{2+} vs 69 μM protein (○); 1.0 mM Ca^{2+} vs 34 μM protein (□); 1.0 mM Ca^{2+} vs 69 μM protein and 1.0 mM NTA (△). (B) 2.0 mM Mg^{2+} vs 66 μM protein (○); 2.0 mM Mg^{2+} vs 65 μM protein and 60 μM EDTA (□). (C) 1.0 mM Ca^{2+} vs 65 μM protein and 1.0 mM Mg^{2+} (○); 1.0 mM Ca^{2+} vs 64 μM protein and 5.0 mM Mg^{2+} (□); 1.0 mM Ca^{2+} vs 61 μM protein and 10.0 mM Mg^{2+} (△). (D) 1.0 mM Ca^{2+} vs 63 μM protein and 60 μM EDTA (○); 1.0 mM Ca^{2+} vs 65 μM protein and 60 μM EGTA (□).

CD sites dictated by local sequence nonidentities? To answer this question, we have examined the consequences of replacing residues 49, 50, 57, 58, 59, and 60 in the CD binding site of rat β-PV with the corresponding residue from CPV3.

The sequence of the engineered CD site in the 49/50/57/58/59/60 variant is nearly identical to that of CPV3. The remaining three nonidentities, at residues 43, 45, and 69, reflect highly conservative amino acid substitutions. At position 43, valine replaces leucine. Both of these apolar side chains terminate in an isopropyl group, so that the impact on core packing is expected to be minor. At position 45, aspartate replaces glutamate. The substitution of one anionic side-chain for another at this solvent-accessible position should likewise have a minimal impact. Finally, at position 69, lysine replaces arginine. Both side chains pair an apolar spacer and a cationic functional group. In the X-ray structure of Ca^{2+}-bound rat β (*34*), the ϵ amino group of Lys-69 is hydrogen-bonded to the side-chain amide carbonyl of Asn-52. The guanidinium group of arginine should function analogously in CPV3. Thus, the behavior of the 49/50/57/58/59/60 variant provides a useful gauge of the relative influence of local and remote structural determinants on the CD site divalent ion-binding signature. In the following paragraphs, we discuss the impact of these rat $\beta \rightarrow$ CPV3 mutations on apoprotein stability and divalent ion affinity.

Conformational Stability. The ratio of $\Delta H_c/\Delta H_{vH}$ is frequently used to diagnose two-state behavior, with values near 1.0 indicating negligible population of intermediate states. Although the ratio obtained for wild-type β (1.07) satisfies this criterion, the four variant proteins exhibit significantly higher values: 1.24 for 49/50, 1.32 for 49/50/57/58, 1.27 for 49/50/57/58/59, and 1.20 for 49/50/57/58/59/60.

The elevated $\Delta H_c/\Delta H_{vH}$ ratios are largely the product of elevated ΔH_c values ($\Delta\Delta H = 14$ kcal/mol). Conceivably, $\beta \rightarrow$ CPV3 mutations at positions 49, 50, 57, 58, 59, and 60, in the overall context of the rat β amino acid sequence, could reduce the cooperativity of the unfolding transition and lead to a greater population of partially folded intermediates. Thus, a concerted effort was made to treat the data for 49/50/57/58 with a three-state model. However, whether the data were subjected to gradient least-squares minimization or Monte Carlo simulation, the quality of the fit was invariably compromised.

In principle, deprotonation events could alter the apparent calorimetric enthalpy. Only two of the six mutations under consideration, D59E and G60E, involve ionizable side-chains. Glu-59 and Glu-60 should be ionized at the pH employed for the study. Moreover, their heats of dissociation would be minimal. Although the mutations could potentially perturb the p*K* values of adjacent residues, there are few candidates that would fit the requisite ionization profile, pro-

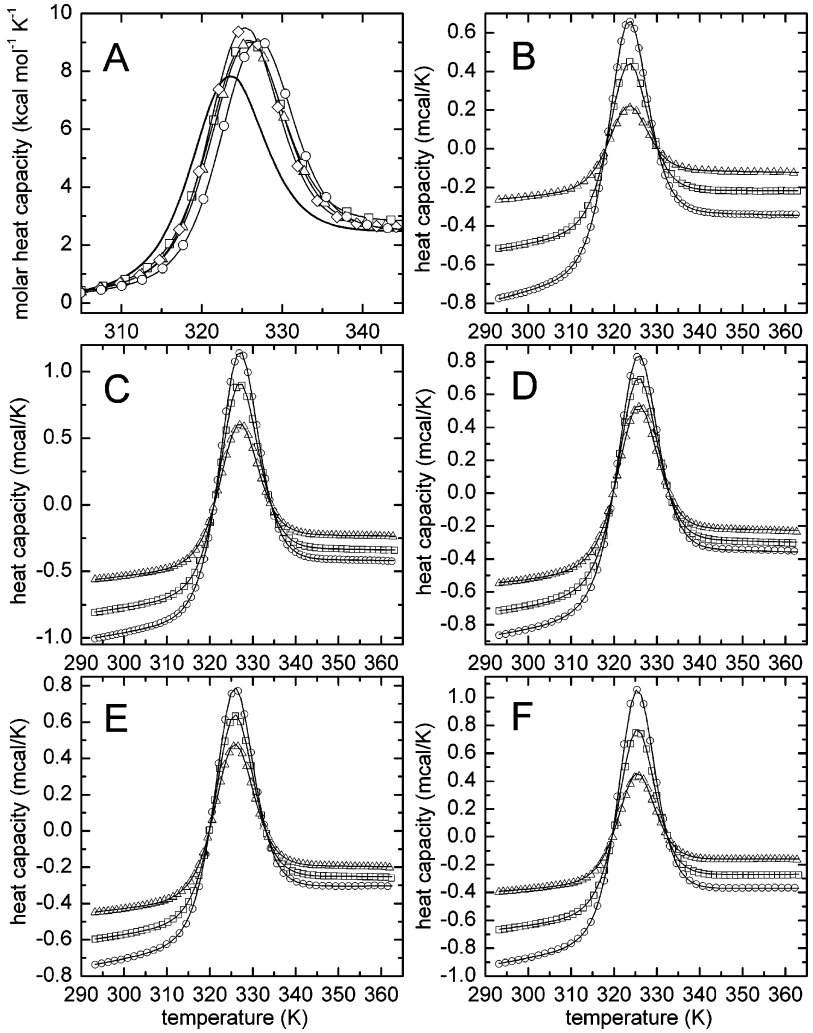

FIGURE 6: Differential scanning calorimetry. (A) Excess molar heat capacity is displayed as a function of temperature for wild-type β-PV (no symbol), β 49/50 (○), β 49/50/57/58 (□), β 49/50/57/58/59 (△), and β 49/50/57/58/59/60 (◇). (B) Heat capacity data for wild-type β at 2.25 (△), 4.49 (□), and 6.73 (○) mg/mL. Solid lines indicate the best global least-squares fit ($\chi_r^2 = 0.84$) to a two-state model. (C) Data for β 49/50 at 4.66 (△), 6.95 (□), and 8.77 (○) mg/mL, with solid lines indicating the best least-squares fit ($\chi_r^2 = 2.18$). (D) Heat capacity data for β 49/50/57/58 at 4.38 (△), 5.75 (□), and 6.94 (○) mg/mL; $\chi_r^2 = 0.99$ for the optimal fit. (E) Heat capacity data for β 49/50/57/58/59 at 3.79 (△), 5.06 (□), and 6.25 (○) mg/mL; $\chi_r^2 = 1.14$. (F) Heat capacity data for β 49/50/57/58/59/60 at 3.29 (△), 5.61 (□), and 7.76 (○) mg/mL; $\chi_r^2 = 1.57$. For clarity, only subsets of the data have been plotted in panels B−F.

Table 3: Summary of DSC Data[a]

protein	T_m	$\Delta\Delta T_m$	ΔH_d	ΔH_{vh}	ΔC_p	$\Delta\Delta G_{conf}$[b]	$\Delta\Delta G_{conf}$[c]
	49.3		72.9	67.9	1.60		
wt rat β[c]							
	49.2, 49.4		72.5, 73.1	67.7, 68.2	1.57, 1.63		
	52.7		86.6	69.9	1.76		
49/50		3.4				0.69	0.20
	52.6, 52.8		86.3, 86.9	69.6, 70.1	1.74, 1.80		
	51.2,		87.0	66.0	1.98		
49/50/57/58		1.9				0.37	−0.43
	51.0, 51.3		86.7, 87.3	65.8, 66.2	1.95, 2.00		
	51.6		86.7	68.3	1.74		
49/50/57/58/59		2.3				0.47	0.04
	51.4, 51.7		86.3, 87.0	68.0 68.5	1.72, 1.77		
	51.2		86.5	72.2	1.70		
49/50/57/58/59/60		1.9				0.53	0.37
	51.1, 51.4		86.2, 86.8	72.1, 72.3	1.69, 1.71		

[a] Temperatures are reported in °C, energies in kcal mol^{-1}, and ΔC_p in kcal mol^{-1} K^{-1}. [b] Apparent changes in conformational stability at 49.3 °C of the wild-type T_m, calculated with eq 3, using the ΔC_p values determined by DSC. [c] Apparent changes in conformational stability at 25 °C, calculated with the ΔC_p estimates from DSC.

tonated in the native state, deprotonated in the denatured state. His-107, if engaged in a salt bridge in the folded protein, is a possibility. However, there are no anionic side chains in the immediate vicinity of the imidazaole ring, at

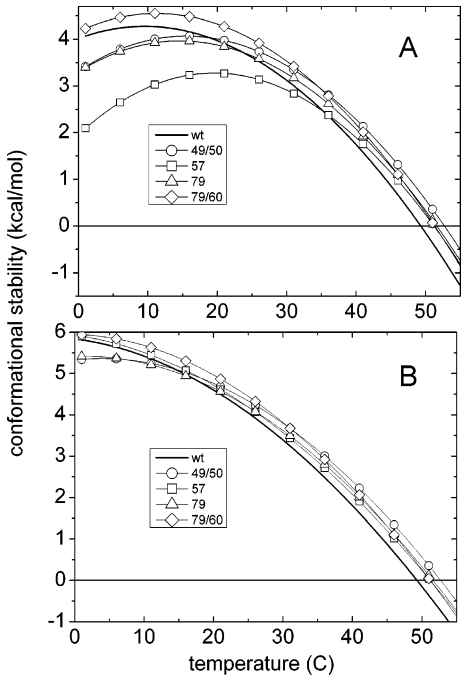

FIGURE 7: Apoprotein stability curves. (A) Conformational stability was calculated as a function of temperature for the apo forms of wild-type β and the four variant proteins, using eq 3 and the estimates of T_m, ΔH_{vH}, and ΔC_p obtained by DSC. Wild-type β, no symbol; 49/50 (○); 49/50/57/58 (□); 49/50/57/58/59 (△); and 49/50/57/58/59/60 (◇). (B) Predicted conformational stabilities, employing the estimate for ΔC_p obtained by global analysis of urea denaturation data collected as a function of temperature. The legend is identical to that in panel A.

least in the crystal structure of Ca^{2+}-bound rat β. Moreover, the enthalpy of ionization of imidazole is just 8.6 kcal/mol (*35*).

Previous studies have indicated that Ca^{2+}-free rat β binds in excess of one equivalent of Na^+. It is known that coupled temperature-dependent binding phenomena can contribute to the apparent energetics of a process (*36*−*38*). Thus, the elevated ΔH_{cal} values might reflect altered monovalent cation binding.

The apparent ΔC_p estimated by DSC increases significantly with the introduction of the F49I and I50L mutations and increases further with the addition of the Y57F and L58I mutations (Table 3). The D59E and G60E mutations reverse the trend observed with 49/50 and 49/50/57/58, producing significant decreases in ΔC_p so that the value determined for the 49/50/57/58/59/60 variant is comparable to that of wild-type β.

At the wild-type T_m (49.3 °C), all four variants exhibit elevated stability, with $\Delta\Delta G_{conf}$ values between 0.37 kcal/mol (for 49/50/57/58) and 0.69 kcal/mol (49/50) (Table 3). Because of the apparent changes in ΔC_p, however, the projected impact of the mutations at 25 °C is variable. 49/50 and 49/50/57/58/59/60 are predicted to be more stable than wild-type β, with $\Delta\Delta G_{conf}$ values of 0.20 and 0.37 kcal/mol, respectively. By contrast, 49/50/57/58 is projected to be 0.43 kcal/mol less stable, and the extrapolated stability of 49/50/57/58/59 is similar to that of the wild type ($\Delta\Delta G_{conf}$ = 0.04 kcal/mol). These predictions are not entirely consistent with urea denaturation studies conducted at 25 °C under comparable solution conditions. Specifically, 49/50/57/58 is found to be slightly more stable than wild-type β (Table 4).

Urea denaturation data collected at 20, 25, 30, and 35 °C were used with the T_m and ΔH_{vH} estimates obtained by DSC to determine effective ΔC_p values for wild-type β and the variant proteins (*31*). The resulting values are lower than those obtained from the DSC analysis (Table 5). Whereas DSC yields a ΔC_p of 1.60 kcal mol^{-1} K^{-1} for wild-type β, global treatment of the urea denaturation data affords a value of 1.14 kcal mol^{-1} K^{-1}. In the case of 49/50/57/58, the difference is even greater, 1.98 kcal mol^{-1} K^{-1} from DSC and 1.05 from chemical denaturation.

The behavior described here is reminiscent of the discrepancy observed (*39*) in the ΔC_p values measured by DSC and chemical denaturation for Sac7d, a DNA-binding protein from *Sulfolobus acidicaldarius*. In that study, the DSC analysis afforded a lower ΔC_p than the chemical denaturation data, 0.50 versus 0.86 kcal mol^{-1} K^{-1}. The difference was subsequently traced to the impact of protonation and anion-binding events on protein folding (*40*). An analogous phenomenon, perhaps involving Na^+ binding, may underlie the behavior described herein.

An analysis of the urea denaturation data suggests that the combined F49I and I50L mutations increase the effective ΔC_p for unfolding from 1.14 to 1.32 kcal mol^{-1} K^{-1}. This change would be consistent with improved side-chain packing and the more effective burial of the apolar surface. Subsequent introduction of the Y57F and L58I mutations into this background returns ΔC_p to a value slightly lower than that of wild-type β. By a parallel argument, this decrease would be consistent with compromised side-chain packing and a relatively less effective burial of the apolar surface in the apoprotein.

The replacement of Asp-59 by glutamate in 49/50/57/58 once more elevates the ΔC_p to a value approaching that of 49/50. The mechanism by which the conservative substitution of a loop residue impacts ΔC_p is not obvious. Given that the side chain of residue 59 occupies the $-x$ position in the CD site ligand array, it is possible that the effect of E59D on ΔC_p is secondary to altered Na^+ binding. It is worth emphasizing that the F57-I58-E59 sequence triad is virtually invariant in the parvalbumin family. The mammalian β isoform is the only exception, replacing F57-I58-E59 with Y57-L58-D59. This high degree of sequence conservation suggests that the correlated presence of E59 with F57-I58 may have functional relevance.

The replacement of Gly-60 by glutamate has no further impact on ΔC_p. In contrast to Asp-59, the identity of residue 60 is not strongly conserved in the β isoforms from different mammalian species. In fact, glutamate is found at this position in the human and guinea pig isoforms (*12*, *41*).

Divalent Ion Binding. The alterations in binding affinity resulting from these mutations are modest. For two of the variants, however, the relatively minor differences in ΔG belie much larger, compensating changes in binding enthalpy and entropy.

F49I/I50L. These mutations improve Ca^{2+} and Mg^{2+} binding by 0.42 and 0.14 kcal/mol, respectively, the result of minor increases in affinity at both the CD and EF sites (Table 2 and Figure 9D). Urea denaturation data collected as a function of temperature indicate that apo-49/50 is 0.29 kcal/mol more stable than wild-type β at 25 °C (Table 5). Because the ΔG for divalent ion binding corresponds to the difference in the energies of the apo and bound states, the

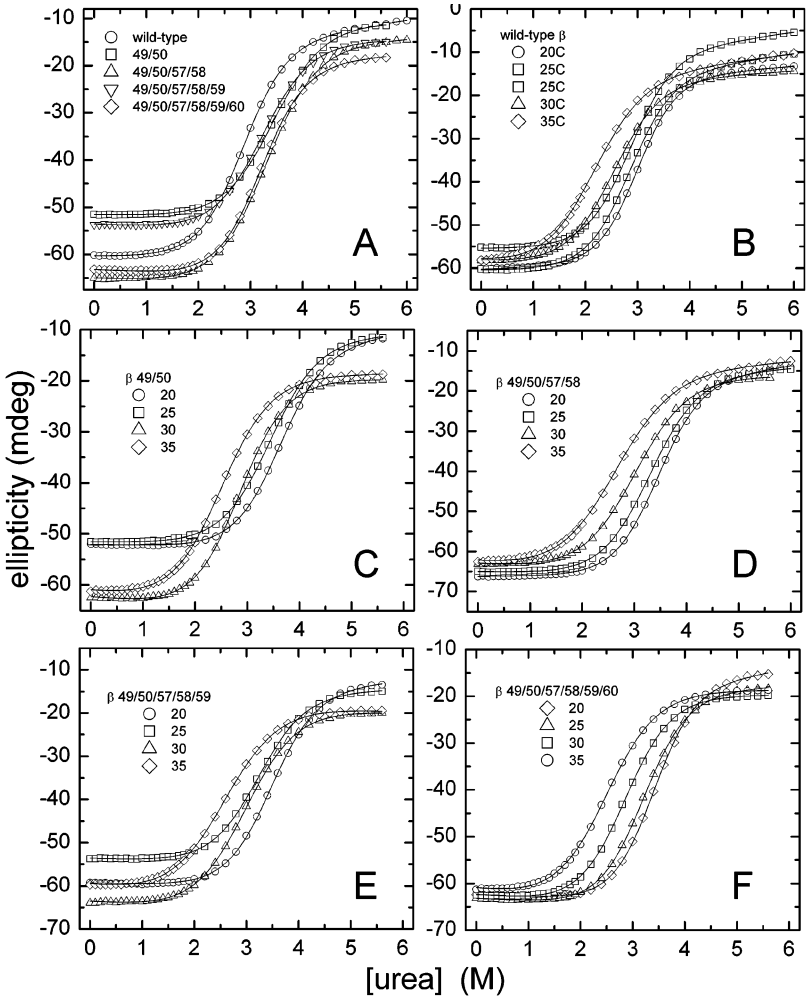

FIGURE 8: Urea denaturation data. (A) Urea-induced denaturation of wild-type β and the four variant proteins at 25 °C. Wild-type, (○); 49/50 (□); 49/50/57/58 (△); 49/50/57/58/59 (▽); and 49/50/57/58/59/60 (◇). (B)−(F) Urea denaturation data collected at 20 (○), 25 (□), 30 (△), and 35 °C (◇) for wild-type β (B), β 49/50 (C), β 49/50/57/58 (D), β 49/50/57/58/59 (E), and β 49/50/57/58/59/60 (F). Duplicate experiments were performed on the wild-type protein at 25 °C.

Table 4: Urea Denaturation Studies at 25 °C

protein	m kcal mol^{-1} M^{-1}	ΔG_o kcal mol^{-1}	$\Delta\Delta G_o$ kcal mol^{-1}
wild-type rat β-PV	1.42 ± 0.02	4.02 ± 0.03	
β 49/50	1.24 ± 0.02	4.26 ± 0.05	0.24
β 49/50/57/58	1.24 ± 0.02	4.06 ± 0.06	0.04
β 49/50/57/58/59	1.28 ± 0.02	4.12 ± 0.05	0.10
β 49/50/57/58/59/60	1.39 ± 0.02	4.43 ± 0.05	0.41

mutations evidently stabilize the Ca^{2+}- and Mg^{2+}-bound states by 0.71 and 0.43 kcal/mol, respectively.

If, as suggested above, the F49I and I50L mutations improve side-chain packing in the apoprotein, metal ion binding might be accompanied by decreased folding. The resulting binding enthalpy would be less exothermic and the conformational entropy penalty less severe. The observed $\Delta\Delta H$ and $-T\Delta\Delta S$ values are consistent with this explanation (+0.83 kcal/mol and −1.25 kcal/mol, respectively, for Ca^{2+}; 2.47 and −2.61 kcal/mol for Mg^{2+}).

F49I/I50L/Y57F/L58I. The combined Y57F and L58I mutations have a differential impact on the Ca^{2+} affinities of the EF and CD sites. Whereas the EF site, relative to 49/50, has a slightly higher Ca^{2+} affinity ($\Delta\Delta G = -0.18$ kcal/mol), the Ca^{2+} affinity of the CD site is reduced ($\Delta\Delta G =$ 0.26 kcal/mol). As a result, there is minimal alteration of the overall free energy change for Ca^{2+} binding (($\Delta\Delta G =$ 0.08 kcal/mol). In contrast to Ca^{2+}, the overall Mg^{2+} affinity of 49/50/57/58 is increased relative to that of 49/50, with perceptible improvements in both binding sites.

The DSC and urea denaturation analyses suggest that the mutations lower ΔH_{vH} by 3.9 kcal/mol and reduce the ΔC_p for denaturation from 1.32 to 1.05 kcal mol^{-1} K^{-1}. These alterations destabilize the apoprotein by 0.15 kcal/mol, relative to that of 49/50. Given the $\Delta\Delta G$ for Ca^{2+} binding of 0.08 kcal/mol, the Ca^{2+}-bound state of 49/50/57/58 must be destabilized by 0.23 kcal/mol.

Earlier, we noted that the reduction in ΔC_p and ΔH_{vH} produced by these mutations would be consistent with less effective side-chain packing in the apoprotein. If correct, divalent ion binding should require a higher degree of protein folding. Consistent with that requirement, the overall Ca^{2+}-binding enthalpy is found to be slightly more favorable ($\Delta\Delta H = -0.43$ kcal/mol), the entropy slightly less favorable ($-T\Delta\Delta S = 0.51$ kcal/mol).

F49I/I50L/Y57F/L58I/D59E. The mammalian β-PV is unique in having aspartate, rather than glutamate, at the $-x$ position in the CD site. Although there was an expectation that this difference might underlie the reduced divalent ion affinity of the CD site, the replacement of D59 by glutamate in wild-type rat β has little effect (*20*) ($\Delta\Delta G = -0.1$ kcal/

Table 5: Urea Denaturation Studies as a Function of Temperature[a]

protein	m(20)	m(25)	m(30)	m(35)	ΔC_p	ΔG_o(25)	$\Delta\Delta G_o$(25)
wild-type rat β-PV	1.54 ± 0.08	1.43 ± 0.01	1.34 ± 0.01	1.25 ± 0.01	1.14 ± 0.03	4.05	
β 49/50	1.33 ± 0.10	1.26 ± 0.01	1.33 ± 0.01	1.27 ± 0.01	1.32 ± 0.02	4.34	0.29
β 49/50/57/58	1.37 ± 0.08	1.28 ± 0.01	1.19 ± 0.01	1.10 ± 0.01	1.05 ± 0.04	4.19	0.14
β 49/50/57/58/59	1.35 ± 0.10	1.30 ± 0.01	1.22 ± 0.01	1.15 ± 0.01	1.26 ± 0.03	4.18	0.13
β 49/50/57/58/59/60	1.47 ± 0.09	1.40 ± 0.01	1.34 ± 0.01	1.25 ± 0.01	1.28 ± 0.03	4.44	0.39

[a] ΔG_o and $\Delta\Delta G_o$ are expressed as kcal/mol and ΔC_p as kcal mol^{-1} M^{-1}. The m values are expressed as kcal mol^{-1} M^{-1}, with the absolute temperature, in Celsius, indicated in parentheses.

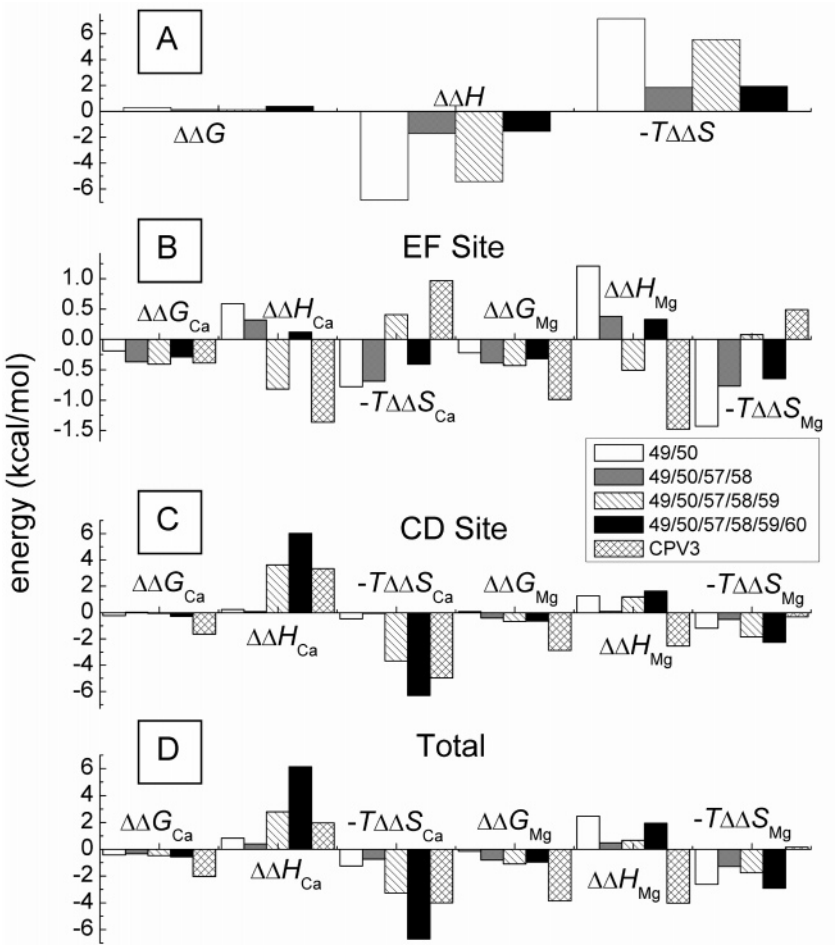

FIGURE 9: Energy diagrams. (A) Alterations in conformational stability, relative to that of wild-type β, for the apo forms of the four β variants at 298 K. (B)−(D) Alterations in the thermodynamic parameters associated with Ca^{2+} and Mg^{2+} binding, relative to that of wild-type β, for the EF site (B), the CD site (C), and both sites (D).

mol). Interestingly, the converse mutation (E59D) in rat α produces a large decrease in Ca^{2+} affinity ($\Delta\Delta G = +1.6$ kcal/mol) (*25*). Thus, the identity of the $-x$ ligand can shape the binding properties of the CD site, but its influence is strongly context-dependent. Producing a $\Delta\Delta G$ of just −0.14 kcal/mol, the impact of D59E in 49/50/57/58 is strongly reminiscent of the behavior observed in wild-type β.

The D59E mutation raises the van't Hoff enthalpy for thermal denaturation by 2.3 kcal/mol and increases the effective ΔC_p by 0.21 kcal mol^{-1} K^{-1}. At 298 K, these changes are nearly compensating so that the stability of 49/50/57/58/59 is very similar to that of 49/50/57/58 ($\Delta\Delta G_{conf} = -0.01$ kcal/mol). Thus, the −0.14 kcal/mol increase in overall Ca^{2+} affinity presumably results from a minor stabilization (0.13 kcal/mol) of the bound state.

The slight improvement in Ca^{2+}-binding free energy, which is associated with the CD site, is accompanied by large, compensating changes in binding enthalpy ($\Delta\Delta H = 3.54$ kcal/mol) and entropy ($-T\Delta\Delta S = -3.68$ kcal/mol). Although the $\Delta\Delta G$ associated with the EF site is negligible, the binding enthalpy is significantly improved ($\Delta\Delta H$ is −1.14 kcal/mol).

The energetics of Mg^{2+} binding are qualitatively similar. The −0.29 kcal/mol improvement in overall binding affinity is produced almost entirely by the second binding event. As with Ca^{2+}, although the $\Delta\Delta G$ associated with the EF site is minute, the binding is significantly more exothermic ($\Delta\Delta H = -0.89$ kcal/mol). Moreover, binding at the CD site is decidedly more endothermic ($\Delta\Delta H = 1.08$ kcal/mol), although the magnitude of the change is less than that for Ca^{2+}.

In Ca^{2+}-bound rat β, water serves as the proximal $-x$ ligand in the CD site, bridging the Ca^{2+} and the carboxylate of Asp-59 (*34*). In all other PVs examined to date, Glu-59

directly coordinates the divalent ion. Thus, the replacement of Asp-59 by glutamate should liberate a water molecule, producing a more favorable binding entropy. The impact of the D59E mutation in 49/50/57/58 closely parallels that observed in wild-type β (*25*). That system likewise exhibits a minor, entropically driven improvement in Ca^{2+} affinity manifested in the CD site binding event, increased exothermicity at the EF site, and decidedly less exothermic CD site binding.

The perturbation of divalent ion binding at the EF site by the D59E mutation, in the CD binding loop, illustrates the structural and thermodynamic linkage between the two PV binding sites. In the bound form, the two Ca^{2+}-binding loops are connected by a short segment of antiparallel β structure, involving residues 57 and 58 in the CD loop and residues 96 and 97 in the EF loop. Although the extent to which this structural element is formed in the apoprotein is unknown, the proximity of the two loops in this region increases the probability that a perturbation of the CD site main-chain dynamics would be transmitted to the EF site.

F49I/I50L/Y57F/L58I/D59E/G60E. The consequences of the G60E mutation resemble those of D59E. Introduction of G60E into 49/50/57/58/59 likewise produces a minor increase in overall Ca^{2+} affinity ($\Delta\Delta G = -0.08$ kcal/mol). Moreover, as in D59E, G60E perturbs the binding properties of both binding sites: a $\Delta\Delta G$ of 0.12 kcal/mol at the EF site and a corresponding value of -0.22 kcal/mol for the CD site. Unlike D59E, however, G60E affords a reduction, albeit minor ($\Delta\Delta G = 0.13$ kcal/mol), in overall Mg^{2+}affinity, resulting from small decreases in the apparent Mg^{2+}-binding constants for both sites.

In further analogy to D59E, the $\Delta\Delta G$ value produced by G60E is accompanied by larger, compensating changes in binding enthalpy and entropy. The $\Delta\Delta H$ values for Ca^{2+} binding at the EF and CD sites are 0.94 and 2.40 kcal/mol, respectively; the corresponding $-T\Delta\Delta S$ values are -0.82 and -2.62 kcal/mol, respectively. The basis for these changes is an interesting cause for speculation. Qualitatively, the energetic signature, positive $\Delta\Delta H$ and negative $-T\Delta\Delta S$, resembles that of the combined F49I/I50L mutations in wild-type β. Recall that those observations were interpreted in terms of improved side-chain packing in the apoprotein. Unlike 49/50, however, the G60E mutation does not afford an increase in the denaturational ΔC_p. Furthermore, the introduction of an additional anionic residue into the anionic CD binding loop is not expected to promote folding.

The thermodynamic perturbation might reflect an alteration in conformational entropy. The replacement of G60 by glutamate should reduce main-chain entropy. To the extent that motion is more restricted in the bound state, the G60E mutation should produce a more favorable $-T\Delta\Delta S$ for Ca^{2+} binding. Matthews et al. (*42*) observed that the G77A substitution in T4 lysozyme produced a 0.4 kcal/mol increase in the ΔG for denaturation, which they attributed to decreased main-chain conformational entropy. It is unlikely, however, that the reduction of main-chain entropy alone could produce the $-T\Delta\Delta S$ value of -3.42 kcal/mol observed for G60E.

The side-chain of E60 might also influence divalent ion-binding energetics. In the structure of Ca^{2+}-bound rat α, the side-chain of Glu-60 is directed away from the bound ion and has no apparent electrostatic interactions with adjacent residues (*34*). However, the carboxylate could conceivably participate in a salt bridge in the apo form. Disruption of that interaction, upon Ca^{2+} binding, would contribute to the observed enthalpic penalty and entropic compensation. Recall that the introduction of the G60E mutation into 49/50/57/58/59 increases the van't Hoff enthalpy for denaturation by 3.9 kcal/mol. That observation would likewise be consistent with the existence of an additional salt bridge in the apoprotein, which is broken upon unfolding.

The G60E mutation has a smaller impact on the underlying thermodynamics of Mg^{2+} binding. The $\Delta\Delta H$ and $-T\Delta\Delta S$ values are just 1.28 and -1.15 kcal/mol, respectively. Spectroscopic (*43*) and structural (*44*) data indicate that the conformational change produced by Mg^{2+} binding is less extensive than that produced by Ca^{2+} binding. Notably, whereas the $-z$ glutamate (E62 in the CD site) coordinates Ca^{2+} in a bidentate manner, it functions as a monodentate ligand to Mg^{2+}. With less extensive rearrangement at the boundary of the CD loop and D helix, the proposed ionic interaction involving E60 in the apoprotein could perhaps be maintained when Mg^{2+} is bound, accounting for the reduction in magnitude of $\Delta\Delta H$ and $-T\Delta\Delta S$.

CONCLUSIONS

Pauls et al. (*45*) produced a variant of rat α-PV in which residues 46, 50, 58, and 66 were replaced by the corresponding residue from rat β. (Note that the L50I and I58L substitutions in that study represent the converse of two mutations included here.) Those four mutations decreased the average Ca^{2+} binding constant from 2.7×10^7 M^{-1} to 1.9×10^7 M^{-1} ($\Delta\Delta G_{Ca} = 0.42$ kcal/mol) and decreased the average microscopic Mg^{2+} binding constant from 4.4×10^4 M^{-1} to 1.9×10^4 M^{-1} ($\Delta\Delta G_{Mg} = 0.99$ kcal/mol). These results are qualitatively consistent with the $\beta \rightarrow$ CPV3 mutations studied herein. Whereas we observe a small increase in Ca^{2+} affinity and slightly larger increase in Mg^{2+} affinity, the converse mutations in rat α produce a small decrease in Ca^{2+} affinity and a somewhat larger decrease in Mg^{2+} affinity.

Incorporating the six site-specific mutations discussed in this paper, the CD site in rat β (residues 41−70) is rendered identical to that of CPV3 at 27 of the 30 residues. Moreover, the remaining three positions reflect highly conservative sequence substitutions. However, the Ca^{2+} and Mg^{2+} affinities of β 49/50/57/58/59/60 remain 1.5 and 2.9 kcal/mol less favorable, respectively, than that of CPV3, and whereas the ΔH associated with Ca^{2+} binding to the CD site in CPV3 is -0.13 kcal/mol, it is 2.56 kcal/mol for the 49/50/57/58/59/60 variant. These findings strongly suggest that residues outside of the CD site EF-hand motif contribute to the unusual divalent ion-binding signature of the mammalian β-parvalbumin isoform.

SUPPORTING INFORMATION AVAILABLE

Divalent ion-binding behavior of β 49/50 and β 49/50/57/58. This material is available free of charge via the Internet at http://pubs.acs.org.

REFERENCES

1. Bootman, M. D., Collins, T. J., Peppiatt, C. M., Prothero, L. S., Mackenzie, L., de Smet, P., Travers, M., Tovey, S. C., Seo, J. T.,

Berridge, M. J., Ciccolini, F., and Lipp, P. (2001) Calcium signalling − an overview, *Semin. Cell Dev. Biol. 12*, 3−10.
2. Berridge, M. J. (2002) The endoplasmic reticulum: a multifunctional signaling organelle, *Cell Calcium 32*, 235−249.
3. Berridge, M. J., Bootman, M. D., and Roderick, H. L. (2003) Calcium signalling: dynamics, homeostasis and remodelling, *Nat. Rev. Mol. Cell Biol. 4*, 517−529.
4. Kretsinger, R. H. (1980) Structure and evolution of calcium-modulated proteins, *CRC Crit. Rev. Biochem. 8*, 119−174.
5. Kawasaki, H., and Kretsinger, R. H. (1995) Calcium-binding proteins 1: EF-hands, *Protein Profile 2*, 297−490.
6. Celio, M. R., Pauls, T., and Schwaller, B. (1996) *Guidebook to the Calcium-Binding Proteins*, Oxford University Press, New York.
7. Kretsinger, R. H., and Nockolds, C. E. (1973) Carp muscle calcium-binding protein. II. Structure determination and general description, *J. Biol. Chem. 248*, 3313−3326.
8. Heizmann, C. W., and Kagi, U. (1989) Structure and function of parvalbumin, *Adv. Exp. Med. Biol. 255*, 215−222.
9. Pauls, T. L., Cox, J. A., and Berchtold, M. W. (1996) The Ca^{2+}-binding proteins parvalbumin and oncomodulin and their genes: new structural and functional findings, *Biochim. Biophys. Acta 1306*, 39−54.
10. Goodman, M., and Pechere, J. F. (1977) The evolution of muscular parvalbumins investigated by the maximum parsimony method, *J. Mol. Evol. 9*, 131−158.
11. Moncrief, N. D., Kretsinger, R. H., and Goodman, M. (1990) Evolution of EF-hand calcium-modulated proteins I. Relationships based on amino acid sequences, *J. Mol. Evol. 30*, 522−562.
12. Fohr, U. G., Weber, B. R., Muntener, M., Staudenmann, W., Hughes, G. J., Frutiger, S., Banville, D., Schafer, B. W., and Heizmann, C. W. (1993) Human α and β parvalbumins. Structure and tissue-specific expression, *Eur. J. Biochem. 215*, 719−727.
13. Novak, R., Brewer, J. M., and Ragland, W. L. (1996) Immunophenotype of splenic lymphocytes with receptors for avian thymic hormone, *FASEB J. 10*, A1048.
14. Novak, R., Henzl, M. T., and Ragland, W. L. (1997) Receptor cells for the CPV3 parvalbumin of chicken thymus in spleen and caecal tonsils, *J. Allergy Clin. Immunol. 99*, S202.
15. Yin, Y., Henzl, M. T., Lorber, B., Nakazawa, T., Thomas, T. T., Jiang, F., Langer, R., and Benowitz, L. I. (2006) Oncomodulin is a macrophage-derived signal for axon regeneration in retinal ganglion cells, *Nature Neurosci. 9*, 843−852.
16. Haiech, J., Derancourt, J., Pechere, J. F., and Demaille, J. G. (1979) Magnesium and calcium binding to parvalbumins: evidence for differences between parvalbumins and an explanation of their relaxing function, *Biochemistry 18*, 2752−2758.
17. Moeschler, H. J., Schaer, J. J., and Cox, J. A. (1980) A thermodynamic analysis of the binding of calcium and magnesium ions to parvalbumin, *Eur. J. Biochem. 111*, 73−78.
18. Henzl, M., and Agah, S. (2006) Divalent ion-binding properties of the two avian β-parvalbumins, *Proteins 62*, 270−278.
19. Hapak, R. C., Zhao, H., Boschi, J. M., and Henzl, M. T. (1994) Novel avian thymic parvalbumin displays high degree of sequence homology to oncomodulin, *J. Biol. Chem. 269*, 5288−5296.
20. Hapak, R. C., Lammers, P. J., Palmisano, W. A., Birnbaum, E. R., and Henzl, M. T. (1989) Site-specific substitution of glutamate for aspartate at position 59 of rat oncomodulin, *J. Biol. Chem. 264*, 18751−18760.
21. Laue, T. M. (1995) Sedimentation equilibrium as a thermodynamic tool, *Methods Enzymol. 259*, 427−452.
22. Haner, M., Henzl, M. T., Raissouni, B., and Birnbaum, E. R. (1984) Synthesis of a new chelating gel: removal of Ca^{2+} ions from parvalbumin, *Anal. Biochem. 138*, 229−234.
23. Henzl, M. T., Agah, S., and Larson, J. D. (2004) Association of the AB and CD-EF domains from rat α- and β-parvalbumin, *Biochemistry 43*, 10906−10917.
24. Henzl, M. T., Agah, S., and Larson, J. D. (2003) Characterization of the metal ion-binding domains from rat α- and β-parvalbumins, *Biochemistry 42*, 3594−3607.
25. Henzl, M. T., Agah, S., and Larson, J. D. (2004) Rat α- and β-parvalbumins: Comparison of their pentacarboxylate and site-interconversion variants, *Biochemistry 43*, 9307−9319.
26. Henzl, M. T., Larson, J. D., and Agah, S. (2003) Estimation of parvalbumin Ca^{2+}- and Mg^{2+}-binding constants by global least-squares analysis of isothermal titration calorimetry data, *Anal. Biochem. 319*, 216−233.
27. Henzl, M. T., Larson, J. D., and Agah, S. (2004) Influence of monovalent cation identity on parvalbumin divalent ion-binding properties, *Biochemistry 43*, 2747−2763.
28. Mabrey, S., and Sturtevant, J. M. (1976) Investigation of phase transitions of lipids and lipid mixtures by high sensitivity differential scanning calorimetry, *Proc. Natl. Acad. Sci. U.S.A. 73*, 3862−3866.
29. Leharne, S. A. and Chowdhry, B. Z. (1998) Thermodynamic Background to Differential Scanning Calorimetry, in *Biocalorimetry: Applications of Calorimetry in the Biological Sciences* (Ladbury, J. E. and Chowdhry, B. Z., Eds.) pp 157−182, John Wiley & Sons, Inc., New York.
30. Santoro, M. M., and Bolen, D. W. (1988) Unfolding free energy changes determined by the linear extrapolation method. 1. Unfolding of phenylmethanesulfonyl α-chymotrypsin using different denaturants, *Biochemistry 27*, 8063−8068.
31. Pace, C. N., and Laurents, D. V. (1989) A new method for determining the heat capacity change for protein folding, *Biochemistry 28*, 2520−2525.
32. Myers, J. K., Pace, C. N., and Scholtz, J. M. (1995) Denaturant m values and heat capacity changes: relation to changes in accessible surface areas of protein unfolding, *Protein Sci. 4*, 2138−2148.
33. Cox, J. A., Milos, M., and MacManus, J. P. (1990) Calcium- and magnesium-binding properties of oncomodulin. Direct binding studies and microcalorimetry, *J. Biol. Chem. 265*, 6633−6637.
34. Ahmed, F. R., Rose, D. R., Evans, S. V., Pippy, M. E., and To, R. (1993) Refinement of recombinant oncomodulin at 1.30 Å resolution, *J. Mol. Biol. 230*, 1216−1224.
35. Fukada, H., and Takahashi, K. (1998) Enthalpy and heat capacity changes for the proton dissociation of various buffer components in 0.1 M potassium chloride, *Proteins 33*, 159−166.
36. Eftink, M. R., Anusiem, A. C., and Biltonen, R. L. (1983) Enthalpy-entropy compensation and heat capacity changes for protein-ligand interactions: general thermodynamic models and data for the binding of nucleotides to ribonuclease A, *Biochemistry 22*, 3884−3896.
37. Ferrari, M. E., and Lohman, T. M. (1994) Apparent heat capacity change accompanying a nonspecific protein-DNA interaction, *Biochemistry 33*, 12896−12910.
38. Kozlov, A. G., and Lohman, T. M. (2000) Large contributions of coupled protonation equilibria to the observed enthalpy and heat capacity changes for ssDNA binding to *Escherichia coli* SSB protein, *Proteins 41*, 23−43.
39. McCrary, B. S., Edmondson, S. P., and Shriver, J. W. (1996) Hyperthermophile protein folding thermodynamics: differential scanning calorimetry and chemical denaturation of Sac7d, *J. Mol. Biol. 264*, 784−805.
40. McCrary, B. S., Bedell, J., Edmondson, S. P., and Shriver, J. W. (1998) Linkage of protonation and anion binding to the folding of Sac7d, *J. Mol. Biol. 276*, 203−224.
41. Henzl, M. T., Shibasaki, O., Comegys, T. H., Thalmann, I., and Thalmann, R. (1997) Oncomodulin is abundant in the organ of Corti, *Hear. Res. 106*, 105−111.
42. Matthews, B. W., Nicholson, H., and Becktel, W. J. (1987) Enhanced protein thermostability from site-directed mutations that decrease the entropy of unfolding, *Proc. Natl. Acad. Sci. U.S.A. 84*, 6663−6667.
43. Blancuzzi, Y., Padilla, A., Parello, J., and Cave, A. (1993) Symmetrical rearrangement of the cation-binding sites of parvalbumin upon Ca^{2+}/Mg^{2+} exchange. A study by ^1H 2D NMR, *Biochemistry 32*, 1302−1309.
44. Declercq, J. P., Tinant, B., Parello, J., and Rambaud, J. (1991) Ionic interactions with parvalbumins. Crystal structure determination of pike 4.10 parvalbumin in four different ionic environments, *J. Mol. Biol. 220*, 1017−1039.
45. Pauls, T. L., Durussel, I., Clark, I. D., Szabo, A. G., Berchtold, M. W., and Cox, J. A. (1996) Site-specific replacement of amino acid residues in the CD site of rat parvalbumin changes the metal specificity of this Ca^{2+}/Mg^{2+}-mixed site toward a Ca^{2+}-specific site, *Eur. J. Biochem. 242*, 249−255.
46. Gillen, M. F., Banville, D., Rutledge, R. G., Narang, S., Seligy, V. L., Whitfield, J. F., and MacManus, J. P. (1987) A complete complementary DNA for the oncodevelopmental calcium-binding protein, oncomodulin, *J. Biol. Chem. 262*, 5308−5312.

BI061421H